Azimuthal Harmonic Coefficients of the Microwave Backscattering From a Non-Gaussian Ocean Surface With the First-Order SSA Model

Christophe Bourlier

Abstract—In this paper, the first-order small slope approximation is applied to a rough sea surface with non-Gaussian statistics, for which the third- and the fourth-order statistics are taken into account in the calculation of the radar cross section. From the Cox and Munk slope distribution, the higher order statistic moments are derived, and behaviors of the corresponding correlation functions are assumed. We show that the fourth order (related to the peakedness or kurtosis) is isotropic, whereas the third order (related to the skewness) has a behavior as $\cos(\psi)$, where ψ is the wave direction along the wind direction. Thus, using the Elfouhaily *et al.* sea height spectrum, related to the second-order statistics, we show that the normalized radar backscattering cross section (NRBCS) can be expanded as an even Fourier series in $\cos(n\phi)$ (where n is a positive integer), for which the harmonic coefficients require only a single integration over the radial distance. This result is consistent with experimental data done for microwave frequencies. In addition, we show for microwave frequencies (like C- and Ku-bands) that the Fourier series can be truncated up to the second order, since the higher order harmonic coefficients vanish. The NRBCS is also compared with empirical backscattering models CMOD2-I3 and SASS-II, valid in C- and Ku-bands, according to the scattering angle and the wind direction. The first-order harmonic coefficient predicts the surface asymmetry along the upwind and downwind directions, whereas the second-order harmonic coefficient describes the surface asymmetry along the upwind and crosswind directions.

Index Terms—Non-Gaussian statistics, ocean remote sensing, radar scattering, scattering from rough surfaces.

I. INTRODUCTION

IN THE LAST three decades, considerable efforts have been devoted to the development of the normalized radar backscattering cross section (NRBCS) to predict and/or to interpret measured data from ocean surfaces. For a multiscale surface like the ocean, to calculate the NRBCS from analytical scattering model, we can use the two-scale model (TSM) [1]–[5], the integral equation method (IEM) model [6], [7], the modified IEM model denoted by the author as IEMM [8], the small slope approximation (SSA) [9]–[13], the weighted curvature approximation (WCA) [14], and the full wave solution [15].

From microwave measurements [16]–[21] for copolarizations [vertical (VV) and horizontal (HH)], the NRBCS is expanded as $\sigma_{pq}(\theta, u, \phi) = \sigma_{pq}^0(\theta, u) + \sigma_{pq}^1(\theta, u)\cos(\phi) + \sigma_{pq}^2(\theta, u)\cos(2\phi)$, which depends on the scattering angle θ, the wind speed u and the azimuthal wind direction ϕ. By analogy with the Fourier series, $\sigma_{pq}^n(\theta, u)$ denotes the n Fourier coefficient. The isotropic backscattering term σ_{pq}^0 mainly carries a piece of information on the wind speed, σ_{pq}^1 is related to the surface asymmetry along the up ($\phi = 0$) and down ($\phi = 180°$) wind directions, and σ_{pq}^2 describes the surface asymmetry along the up ($\phi = 0$) and cross ($\phi = 90°$) wind directions. Assuming a Gaussian process, from the first-order SSA model, in [10], [13], σ_{pq}^0 and σ_{pq}^2 are calculated analytically, which require only a single numerical integration over the radial distance between two points on the surface (the surface is assumed to be stationary). In addition, they showed that σ_{pq}^1 is equal to zero because the sea surface statistics are assumed to be Gaussian.

The contribution of σ_{pq}^1 is attributed to the hydrodynamic modulation of the short waves by the longer ones. For instance, under moderate wind conditions, the crests of the waves are tilted toward the wind direction. This point has been studied both theoretically and experimentally by Longuet-Higgins [22] within the introduction of the higher order statistics. With the IEM approach, Fung and Chen [6], [7] included the surface statistics up to the third order, which is related to the surface skewness (or the bispectrum), in the NRBCS calculation. This allows one to predict the upwind/downwind asymmetry phenomenon. We can also quote the work of Elfouhaily *et al.* [23]. Nickolaev *et al.* [5] applied the two-scale model to sea surfaces whose slope probability density function is described as the Gram–Charlier type truncated up to the fourth order. The higher order statistical moments are obtained from the Cox and Munk slope distribution [24]. Recently, McDaniel introduced the skewness and the peakedness (related to the fourth-order statistical moment) effects in the calculation of the NRBCS obtained from the full wave method.

To our knowledge, no published paper has presented a simple expression of the nth Fourier coefficients $\{\sigma_{pq}^n(\theta, u)\}$ and has justified the use of an expansion of NRBCR as the even Fourier series along the wind direction. It is the purpose of this paper. From the first-order SSA model, we show that $\{\sigma_{pq}^n(\theta, u)\}$ can be computed from a one-dimensional integral, where both the skewness and the peakedness effects are taken into account. In addition, they are compared with microwave experimental data, where the height roughness spectrum is given by Elfouhaily *et al.* [25], and the higher order statistics are performed from the Cox and Munk slope distribution.

The paper is organized as follows. The second section presents the first-order SSA model, where the skewness and the peaked-

ness effects are accounted for the derivation of the ensemble average over the surface heights (this leads to the derivation of the characteristic function of two variables). In Section III, from the Cox and Munk slope distribution, the higher order statistical moments are derived. This allows us to find the symmetry properties of the skewness and the peakedness correlation functions along the wind direction and to perform the angular integration with the help of the Bessel functions. The last section studies the skewness and the peakedness effects on the NRBCS and compares the model with microwave measurements.

II. SCATTERING MODEL

The small-slope approximation is appropriate for scattering from both large- (the high-frequency regime), intermediate- and small-scale (the low-frequency regime) roughness scales within a single theoretical scheme. Both the lowest order approximation (denoted as SSA-1) and the next-order approximation (referred to as SSA-2), which is a correction of the lowest order one, can be calculated. The SSA was verified in a great number of numerical simulations [10]–[13], [26]–[28].

Assuming a statistically Gaussian sea surface, Voronovich *et al.* [11, Fig. 1(e) and (f)] compared SSA-1 with $\mathrm{SSA}{-}1 + \mathrm{SSA}{-}2$ for a radar frequency $f = 14$ GHz, for wind speeds $u_{10} = \{5, 15\}$ m/s (defined as 10 m above the sea), and for scattering angles $\theta \in [0°; 60°]$. They observed that the mean backscattering coefficients are similar for the VV polarization, whereas for the HH polarization, the difference between $\mathrm{SSA}{-}1 + \mathrm{SSA}{-}2$ and SSA-1 increases with the wind speed, but remains within about 1 dB. In addition, for $u_{10} = \{5, 15\}$ m/s and $f = 5.3$ GHz, McDaniel [12, Figs. 4 and 5] observed a deviation between $\mathrm{SSA}{-}1 + \mathrm{SSA}{-}2$ and SSA-1 smaller than 1 dB. Therefore, for radar microwave backscattering, SSA-1 can be used with a mean accuracy of the order of 1 dB. It must be noted that the purpose of this paper is to obtain simple mathematical expressions of the azimuthal harmonic coefficients $\{\sigma_{pq}^n(\theta, u)\}$. Indeed, this is only possible with SSA-1, since the computation of the SSA-2 contribution requires two additional numerical integrations. In addition, SSA-2 is derived only for Gaussian statistics.

With SSA-1, the bistatic scattering coefficient is expressed as [11]

$$\sigma_{pq}^I(\mathbf{k}_i, \mathbf{k}_s) = \frac{1}{\pi} \left| \frac{2q_i q_s B_{pq}(\mathbf{k}_i, \mathbf{k}_s)}{Q} \right|^2 \int \exp[j(\mathbf{k}_s - \mathbf{k}_i) \cdot \mathbf{r}] \\ \cdot \langle \exp[jQ(z_2 - z_1)] \rangle \, d\mathbf{r} \quad (1)$$

where $Q = q_i + q_s$, $\{\mathbf{k}_i, \mathbf{k}_s\}$ the horizontal projections of the incident and scattered wave vectors and $\{q_i, q_s\}$ their vertical projections, respectively. $\{z_1, z_2\}$ are the heights at two arbitrary points on the surface separated by the horizontal distance $\|\mathbf{r}\|$ (the surface is assumed to be stationary). $B_{pq}(\mathbf{k}_i, \mathbf{k}_s)$ is the 2×2 matrix of the first-order small perturbation method given in the Appendix of [11]. The symbol $\langle \cdots \rangle$ stands for the ensemble average over the random variables $\{z_1, z_2\}$. In the backscattering direction, $\mathbf{k}_s = -\mathbf{k}_i, q_s = q_i$ and $B_{VH}(\mathbf{k}_i, -\mathbf{k}_i) = B_{HV}(\mathbf{k}_i, -\mathbf{k}_i)$ vanish, which means that the cross-polarization contributions cannot be predicted. The SSA-2 contribution must then be computed.

For a non-Gaussian surface, Longuet-Higgins [22] showed that the ensemble average is given by successive sums of a Gram–Charlier series defined as

$$\langle \exp[jQ(z_2 - z_1)] \rangle = \exp \left[\sum_{(n,m) \neq (0,0)} \frac{\kappa_{nm}(-jQ)^n(jQ)^m}{n!m!} \right] \\ = \sum_{p=0}^{p=\infty} \frac{1}{p!} \left[\sum_{(n,m) \neq (0,0)} \frac{\kappa_{nm}}{n!m!} \right. \\ \left. \cdot (-jQ)^n(jQ)^m \right]^p. \quad (2)$$

In the above equation, $\kappa_{nm}(\mathbf{r})$ are the statistical cumulants equal for a random process with zero mean values $(\mu_{01} = \mu_{10} = 0)$ to the statistical moments $\mu_{nm}(\mathbf{r})$ defined as

$$\mu_{nm}(\mathbf{r}) = \langle z_1^n z_2^m \rangle = \int z_1^n z_2^m p_z(z_1, z_2) \, dz_1 \, dz_2. \quad (3)$$

$p_z(z_1, z_2)$ is the height joint probability. To be consistent with the slope distribution of the Cox and Munk given in the next section, the double sum in (2) is expanded up to $n + m \leq 4$. We then obtain

$$\langle \exp[jQ(z_2 - z_1)] \rangle \approx \exp \left\{ -Q^2 \left[\frac{1}{2}(\mu_{02} + \mu_{20}) - \mu_{11} \right] \right. \\ - \frac{jQ^3}{6} [\mu_{03} - \mu_{30} + 3(\mu_{21} - \mu_{12})] \\ + \frac{Q^4}{24} [\mu_{04} + \mu_{40} \\ \left. - 4(\mu_{31} - \mu_{13}) + 6\mu_{22}] \right\}. \quad (4)$$

We can note that $\mu_{02} = \mu_{20} = \sigma_z^2, \mu_{03} = \mu_{30} = 0$ and $\mu_{04} = \mu_{40} = 3\sigma_z^2$, where σ_z^2 is the height variance. $W_2 = \langle z_1 z_2 \rangle$ denotes the well-known height correlation function, whereas $\mu_{21} = \langle z_1 z_2^2 \rangle$ is referred to as the bicorrelation function. The bicorrelation function can be split up into a symmetric part W_{3s} $(W_{3s}(-\mathbf{r}) = W_{3s}(\mathbf{r}))$ and an asymmetric part W_3 $(W_3(-\mathbf{r}) = -W_3(\mathbf{r}))$, where $W_{3s} = (\mu_{12} + \mu_{21})/2$ and $W_3 = (\mu_{12} - \mu_{21})/2$. Chen, Fung *et al.* [6], [7] denoted W_3 as the skewness function, because it is related to the surface asymmetry. In addition, the peakedness function [29] related to the fourth-order statistical is expressed as $W_4 = \langle (z_1 - z_2)^4 \rangle/12$, which is an even function $(W_4(-\mathbf{r}) = W_4(\mathbf{r}))$. The definition of W_4 is such that $W_4(\infty) = \sigma_z^4$ and $W_4(\mathbf{0}) = 0$. From (4), the resulting equation is then

$$\langle \exp[jQ(z_2 - z_1)] \rangle \approx \exp \left[-Q^2 (\sigma_z^2 - W_2) \right] \\ \cdot \exp \left\{ jQ^3 W_3 + \frac{Q^4}{2} \left[W_4 - (\sigma_z^2 - W_2)^2 \right] \right\} \\ \cdot \exp \left[\frac{Q^4}{2} (\sigma_z^2 - W_2)^2 \right]. \quad (5)$$

In the right-hand side, the first exponential term is equal to the height joint characteristic function of a Gaussian process, whereas the second and the third exponential terms are related to the non-Gaussian effect of the surface. For a Gaussian process, $W_4 = (\sigma_z^2 - W_2)^2$ and $W_3 = 0$, which means that the second exponential term is equal to one. In addition, to be consistent

with the expansion of order Q^4 in (2), the third exponential term must equal to one. Thus, we find the well-known result $\langle \exp[jQ(z_2 - z_1)] \rangle = \exp[-Q^2(\sigma_z^2 - W_2)]$ and (5) becomes with $W_{4d} = W_4 - (\sigma_z^2 - W_2)^2$ (this function measures the deviation of the peakedness function between surfaces statistically non-Gaussian and Gaussian)

$$\langle \exp[jQ(z_2 - z_1)] \rangle \approx \exp\left[-Q^2\left(\sigma_z^2 - W_2\right)\right]$$
$$\cdot \exp\left(jQ^3 W_3 + \frac{Q^4 W_{4d}}{2}\right). \quad (6)$$

III. DERIVATIONS OF THE HIGHER ORDER STATISTICS

The ensemble average requires the knowledge of the height correlation function $W_2(\mathbf{r})$, the skewness function $W_3(\mathbf{r})$ and the deviated peakedness function $W_{4d}(\mathbf{r})$. The height correlation function is obtained from the height roughness spectrum, which is related to the height and slope rms. The higher order statistics cannot then be calculated from the height spectrum. Nevertheless, as the Cox and Munk slope probability involves statistics up to fourth order, $W_3(\mathbf{r})$ and $W_{4d}(\mathbf{r})$ can be derived for $\|\mathbf{r}\|$ close to zero. For any $\|\mathbf{r}\|$, $W_3(\mathbf{r})$ and $W_{4d}(\mathbf{r})$ are derived by assuming an extrapolation. It is important to note that the slope probability gives only information over the statistical moments of the surface, such its rms slope, its skewness and its kurtosis, and the corresponding spectra or correlations have to be known to obtain a full description of the surface statistic features.

A. Second-Order Statistic

We assume that the sea surface height obeys the Elfouhaily et al. [25] directional spectrum, $\hat{W}_2$. In polar coordinates, $\mathbf{k} = (k_x, k_y) = (k\cos\psi, k\sin\psi)$, it is defined as $(\hat{W}_2(\mathbf{k})d\mathbf{k} = k \times \hat{W}_2(k,\psi)dkd\psi)$

$$\hat{W}_2(k,\psi) = \hat{W}_{20}(k)[1 + \hat{\Delta}(k)\cos(2\psi)]/(2\pi) \quad (7)$$

where $\hat{W}_{20}(k)$ represents the isotropic part of the sea spectrum and $\hat{\Delta}(k)$ is the spreading function. The sea height correlation function is then expressed in polar coordinates, $\mathbf{r} = (r_x, r_y) = (r\cos\Phi, r\sin\Phi)$, as [13], [30]

$$W_2(r,\Phi) = W_{20}(r) - W_{22}(r)\cos(2\Phi) \quad (8)$$

where

$$W_{20}(r) = \int_0^\infty \hat{W}_{20}(k)J_0(rk)\,dk \quad (9a)$$

$$W_{22}(r) = \int_0^\infty \hat{W}_{20}(k)\hat{\Delta}(k)J_2(rk)\,dk. \quad (9b)$$

$W_{20}(r)$ is the isotropic part, whereas $W_{22}(r)$ denotes the anisotropic part. J_n is the nth-order Bessel function of the first kind. It must noted that $W_2(r, \Phi + \pi) = W_2(r, \Phi)$ which explains that the upwind/downwind asymmetry cannot be predicted. On the other hand, since $W_2(r, \Phi + \pi/2) \neq W_2(r, \Phi)$ the upwind/crosswind asymmetry is predicted.

B. Third- and Fourth-Order Statistic Moments for r Close to Zero

To determine the symmetry properties of $W_3(\mathbf{r})$ and $W_{4d}(\mathbf{r})$, we can use the slope distribution of the Cox and Munk [24] given by

$$p_s(\gamma_x, \gamma_y) = \frac{1}{2\pi\sigma_{sx}\sigma_{sy}} \exp\left(-\frac{\gamma_x^2}{2\sigma_{sx}^2} - \frac{\gamma_y^2}{2\sigma_{sy}^2}\right)$$
$$\cdot \left[1 + \frac{c_{21}}{2}\left(\Gamma_y^2 - 1\right)\Gamma_x + \frac{c_{03}}{6}\left(\Gamma_x^2 - 3\right)\Gamma_x\right.$$
$$+ \frac{c_{22}}{4}\left(\Gamma_x^2 - 1\right)\left(\Gamma_y^2 - 1\right) + \frac{c_{40}}{24}\left(\Gamma_y^4 - 6\Gamma_y^2 + 3\right)$$
$$+ \left.\frac{c_{04}}{24}\left(\Gamma_x^4 - 6\Gamma_x^2 + 3\right)\right] \quad (10)$$

where

$$\Gamma_{x,y} = \frac{\gamma_{x,y}}{\sigma_{sx,sy}} \quad \begin{cases} \sigma_{sx}^2 = (3.16u_{12} \pm 4)10^{-3} \\ \sigma_{sy}^2 = (1.92u_{12} + 3 \pm 4)10^{-3} \end{cases} \quad (11a)$$

$$\begin{cases} c_{21} = (0.86u_{12} - 1 \pm 3)10^{-2} \geq 0 \\ c_{03} = (3.3u_{12} - 4 \pm 12)10^{-2} \geq 0 \end{cases} \quad (11b)$$

$$\begin{cases} c_{04} = 0.23 \pm 0.41 \\ c_{40} = 0.40 \pm 0.23 \\ c_{22} = 0.12 \pm 0.06. \end{cases} \quad (11c)$$

The wind speed u_{12} is measured at 12.5 m above the sea. $\{\gamma_x, \gamma_y\}$ are the surface slopes in the up- and cross-wind directions and $\{\sigma_{sx}^2, \sigma_{sy}^2\}$ are their variances, respectively. The important results of $p(\gamma_x, \gamma_y)$ are reported in [24] and [31]. The characteristic function of the slopes is then

$$\left\langle e^{jQ(x\gamma_x + y\gamma_y)} \right\rangle = \int p(\gamma_x, \gamma_y) e^{jQ(x\gamma_x + y\gamma_y)}\,d\gamma_x\,d\gamma_y$$
$$= \exp\left[-\frac{Q^2}{2}\left(\sigma_{sx}^2 x^2 + \sigma_{sy}^2 y^2\right)\right]$$
$$\cdot \left[1 - \frac{jQ^3}{6} x\sigma_{sx}\left(x^2\sigma_{sx}^2 c_{03} + 3y^2\sigma_{sy}^2 c_{21}\right)\right.$$
$$+ \frac{Q^4}{24}\left(x^4\sigma_{sx}^4 c_{04} + y^4\sigma_{sy}^4 c_{40}\right.$$
$$\left.\left. + 6x^2 y^2 \sigma_{sx}^2 \sigma_{sy}^2 c_{22}\right)\right]. \quad (12)$$

For r close to zero, we have $z_2 - z_1 \approx \gamma_x x + \gamma_y y$ and $\sigma_z^2 - W_2 \approx (x^2\sigma_{sx}^2 + y^2\sigma_{sy}^2)/2$ (since W_2 is even, we have for $r = 0$, $\partial_{1,0}(W_2) = 0$, $\partial_{0,1}(W_2) = 0$, $\partial_{2,0}(W_2) = -\sigma_{sx}^2$ and $\partial_{0,2}(W_2) = -\sigma_{sy}^2$ where $\partial_{n,m} = \partial^{n+m}/\partial x^n \partial y^n$). Thus, from (6), we obtain

$$\lim_{r \to 0}\langle \exp[jQ(z_2 - z_1)]\rangle \approx \langle \exp[jQ(\gamma_x x + \gamma_y y)]\rangle$$
$$\approx \exp\left[-\frac{Q^2}{2}\left(\sigma_{sx}^2 x^2 + \sigma_{sy}^2 y^2\right)\right]$$
$$\cdot \left(1 + jQ^3 W_3 + \frac{Q^4 W_{4d}}{2}\right). \quad (13)$$

The comparison of (13) with (12) leads for $r \to 0$ to

$$\begin{cases} W_3(\mathbf{r}) = -\frac{1}{6} x\sigma_{sx}\left(x^2\sigma_{sx}^2 c_{03} + 3y^2\sigma_{sy}^2 c_{21}\right) \\ W_{4d}(\mathbf{r}) = \frac{1}{12}\left(x^4\sigma_{sx}^4 c_{04} + y^4\sigma_{sy}^4 c_{40} + 6x^2 y^2\sigma_{sx}^2\sigma_{sy}^2 c_{22}\right). \end{cases} \quad (14)$$

As mentioned by [15], [23], and [32], from (11) we have $3\sigma_{sy}^2 c_{21} \approx \sigma_{sx}^2 c_{03}, \sigma_{sx}^4 c_{04} \approx \sigma_{sy}^4 c_{40} \approx 3\sigma_{sx}^2 \sigma_{sy}^2 c_{22}$. The above equation becomes then in polar coordinates (r, Φ) for $r \to 0$

$$\begin{cases} W_3(r, \Phi) = -r^3 \cos(\Phi)\sigma_{sx}^3 c_{03}/6 \\ W_{4d}(r) = r^4 \sigma_{sx}^2 \sigma_{sy}^2 c_{22}/4. \end{cases} \quad (15)$$

Unlike the height correlation function W_2, we have $W_3(r, \Phi + \pi) = -W_3(r, \Phi)$. We will then show in the next section, that an angular dependence in $\cos(\Phi)$ of W_3 can predict the upwind/downwind asymmetry of the NRBCS, $\sigma_{pq}(\mathbf{k}_i, -\mathbf{k}_i)$. Since $W_3(\mathbf{r})$ is an odd function and $\{W_2(\mathbf{r}), W_4(\mathbf{r})\}$ are even functions ($W_{4d} = W_4 - (\sigma_z^2 - W_2)^2$ is even), we have

$$\partial_{n,m}(W_3)|_{\mathbf{r}=\mathbf{0}} = 0, \quad \text{for} \begin{cases} n \text{ and } m \text{ even} \\ n \text{ and } m \text{ odd} \end{cases} \quad (16)$$

$$\partial_{n,m}(W_{4d})|_{\mathbf{r}=\mathbf{0}} = 0, \quad \text{for} \begin{cases} n \text{ odd and } m \text{ even} \\ n \text{ even and } m \text{ odd} \end{cases} \quad (17)$$

where $\partial_{n,m} = \partial^{n+m}/\partial x^n \partial y^n$. In addition we can note from (15) that

$$\partial_{n,m}(W_3)|_{\mathbf{r}=\mathbf{0}} = 0, \quad \text{for } 0 \le n+m \le 2 \quad (18)$$

$$\partial_{n,m}(W_{4d})|_{\mathbf{r}=\mathbf{0}} = 0, \quad \text{for } 0 \le n+m \le 3. \quad (19)$$

This result is consistent with [6], [7], and [29], where it was shown for a one-dimensional surface that $\{W_{3,4}\}$ must obey $W_3(0) = W_3'(0) = W_3''(0) = 0$ and $W_4(0) = W_4'(0) = W_4''(0) = W_4'''(0) = 0$ to have finite values of the statistical moments. Moreover, since $W_{4d} = W_4 - (\sigma_z^2 - W_2)^2$ and W_2 is an even function, W_{4d} has the same symmetry properties as W_4. We can also note from (15) that

$$\begin{cases} \partial_{3,0}(W_3)|_{\mathbf{r}=\mathbf{0}} = -\sigma_{sx}^3 c_{03} \\ \partial_{1,2}(W_3)|_{\mathbf{r}=\mathbf{0}} = -\sigma_{sx}^3 c_{03}/3 \\ \partial_{0,3}(W_3)|_{\mathbf{r}=\mathbf{0}} = \partial_{2,1}(W_3)|_{\mathbf{r}=\mathbf{0}} = 0 \end{cases} \quad (20)$$

$$\begin{cases} \partial_{4,0}(W_{4d})|_{\mathbf{r}=\mathbf{0}} = 6\sigma_{sx}^2 \sigma_{sy}^2 c_{22} \\ \partial_{0,4}(W_{4d})|_{\mathbf{r}=\mathbf{0}} = 6\sigma_{sx}^2 \sigma_{sy}^2 c_{22} \\ \partial_{2,2}(W_{4d})|_{\mathbf{r}=\mathbf{0}} = 2\sigma_{sx}^2 \sigma_{sy}^2 c_{22} \\ \partial_{1,3}(W_{4d})|_{\mathbf{r}=\mathbf{0}} = \partial_{3,1}(W_{4d})|_{\mathbf{r}=\mathbf{0}} = 0. \end{cases} \quad (21)$$

We then observe that (21) is consistent with (17). However, (16) cannot predict that $\partial_{0,3}(W_3)|_{\mathbf{r}=\mathbf{0}}$ and $\partial_{2,1}(W_3)|_{\mathbf{r}=\mathbf{0}}$ vanish since n is even and m is odd. This is due to the fact that $W_3 \cong r^4 \cos \Phi \cong x f(r)$ where f is a function of r. Thus, we can show for any f that the behavior as $\cos \Phi$ implies that $\partial_{0,3}(W_3)|_{\mathbf{r}=\mathbf{0}}$ and $\partial_{2,1}(W_3)|_{\mathbf{r}=\mathbf{0}}$ vanish.

C. Skewness and Deviated Peakedness Functions for Any r

To have a complete description of $\{W_{3,4d}(\mathbf{r})\}$, (15) must be both extrapolated for any $\mathbf{r}$ and must satisfy the symmetry properties given by (16)–(21). Unfortunately, there are poor experimental data in the literature on the skewness and peakedness functions for ocean rough surfaces. Fung and Chen et al. selected the following form of the skewness function $W_3(r, \Phi) = \alpha_1(r \cos \Phi)^3 \exp(-r^{\alpha_2}/\alpha_3)$ where $\{\alpha_1 = \sigma_z^{-3}, \alpha_2 = 2, \alpha_3 = s_0^2\}$ [6], $\{\alpha_1 = \sigma_z^{-3}, \alpha_2 = 1, \alpha_3 = s_0\}$ [33], and $\{\alpha_1 = s_0^{-3}, \alpha_2 = 2, \alpha_3 = s_0^2\}$ [7], [34]. Guissard [29] pointed out that the determination of α_3, which is proportional to the skewness correlation length, is not based on direct measurements of the skewness. It has seemingly been selected in such a way that the NRBCS agrees with measurements. In

addition, we can note that $W_3(r, \Phi) \cong (\cos \Phi)^3$ instead of $\cos \Phi$. McDaniel [15] assumed that the roughness spectrum of $\{W_{3,4d}(\mathbf{r})\}$, denoted as $\{\hat{W}_{3,4d}(\mathbf{k})\}$, have the following forms $\hat{W}_{3,4d}(k, \psi) = \hat{W}_{20}(k)\hat{F}_{3,4d}(k, \psi)/(2\pi)$, where $\hat{W}_{20}(k)$ stands for the isotropic part of the sea height spectrum, given by the Elfouhaily et al. model, and $\hat{F}_{3,4d}(k, \psi)$ are the anisotropic parts of the skewness and deviated peakedness spectra. These functions are determined from the properties given in the previous subsection. This solution is not adopted because $\{W_{3,4d}(r, \Phi)\}$ have to be reevaluated from $\{\hat{W}_{3,4d}(k, \psi)\}$ for the calculation of the NRBCS. However, in this paper, we use a combination of the two previous approaches.

To have the properties given by (16)–(21), we assume the following forms of $\{W_{3,4d}(r, \Phi)\}$

$$W_3(r, \Phi) = W_{30}(r) \cos \Phi$$

where

$$W_{30}(r) = -\sigma_{zS}^3 \frac{r^3}{L_{c3}^3} \exp\left(-\frac{r^2}{L_{c3}^2}\right) \quad (22)$$

$$\frac{W_{4d}(r)}{\sigma_{zL}^4} = \frac{r^4}{L_{c4}^4} \exp\left(-\frac{r^4}{L_{c4}^4}\right). \quad (23)$$

The definition of W_{4d} is such as $W_{4d}(0) = W_{4d}(\infty) = 0$. Moreover they obey the conditions expressed from (18)–(21). Thus

$$\partial_{3,0}(W_3)|_{\mathbf{r}=\mathbf{0}} = -\sigma_{sx}^3 c_{03} = \frac{6\sigma_{zS}^3}{L_{c3}^3}$$

$$\Rightarrow L_{c3} = \left(\frac{6}{c_{03}}\right)^{1/3} \frac{\sigma_{zS}}{\sigma_{sx}} \quad (24)$$

$$\partial_{4,0}(W_{4d})|_{\mathbf{r}=\mathbf{0}} = 6\sigma_{sx}^2 \sigma_{sy}^2 c_{22} = \frac{24\sigma_{zL}^4}{L_{c4}^4}$$

$$\Rightarrow L_{c4} = \sigma_{zL} \left(\frac{2}{\sigma_{sx}\sigma_{sy}\sqrt{c_{22}}}\right)^{1/2}. \quad (25)$$

The Cox and Munk measurements indicate that an oil slick, which tends to suppress the capillary waves (small scale), reduces the skewness but leaves the deviated peakedness unchanged. This means that the skewness is related to the small scale of height rms σ_{zS}, whereas the peakedness is related to the large scale of height rms σ_{zL}. Thus, in (24) and (25), the rms height is not the same. The total height variance can be split up as

$$\sigma_z^2 = \sigma_{zL}^2 + \sigma_{zS}^2$$
$$= \int_0^{K_S} \hat{W}_{20}(k)\, dk + \int_{K_S}^{\infty} \hat{W}_{20}(k)\, dk \quad (26)$$

where the cutoff wavenumber K_S, which separates the small and the large scales, must be determined. Its calculation is difficult since few results exist in the literature. Guissard [29] set $\sigma_{zS} = K_0/\delta(u_{10})$ where K_0 is the incident electromagnetic wavenumber, and δ depends on the wind speed. In the X-band ($f = 10$ GHz), Elfouhaily et al. [23] set $K_S = 50$ rad/m. Thus, these two approaches suggest that σ_{zS} is dependent of the radar frequency, which is surprising since σ_{zS} is an intrinsic parameter of the sea. We then propose the following method to estimate σ_{zS}. Since an oil slick sea suppresses the capillary waves,
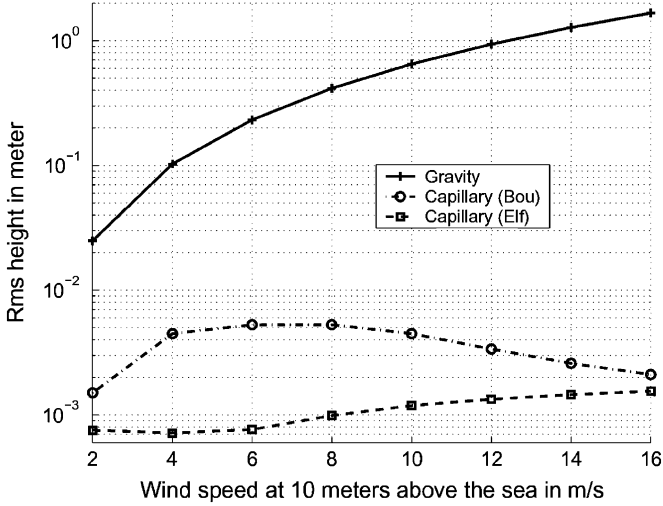
Fig. 1. RMS height versus the wind speed u_{10}.

Fig. 2. Correlation lengths in meters of the height L_{c2}, of the skewness L_{c3} (according to two approaches), and of the deviated peakedness L_{c4} versus the wind speed u_{10}.

we have for the total slope $\sigma_{sL}^2 = \sigma_{sxL}^2 + \sigma_{syL}^2$ of the gravity waves

$$\sigma_{sL}^2 = \int_0^{K_S} \hat{W}_{20}(k)k^2 \, dk \approx (1.62u_{12} + 8)10^{-3} \qquad (27)$$

from the Cox and Munk model. When the cumulative integral over K_S reaches the value of the total slope variance of the gravity waves, K_S is determined. For instance, for $u_{10} = \{5, 10, 15\}$ m/s ($u_{12} \approx u_{10}$ with an error of 2%), we obtain $K_S = \{9, 10, 28\}$ rad/m, which is smaller than the value used by Elfouhaily [23]. In addition, we have $\sigma_{zL}/\sigma_z = \{0.999\,47, 0.999\,98, 0.999\,99\}, \sigma_{zS}/\sigma_z = \{0.032\,45, 0.006\,91, 0.001\,58\}$ $((\sigma_{zL}/\sigma_z)^2 + (\sigma_{zS}/\sigma_z)^2 = 1)$, $K_S/K_p = \{33, 147, 915\}$, where K_p is the wavenumber for which the height gravity spectrum reaches its maximum. As shown in [30], only the gravity waves contribute to the height rms, which explains that $\sigma_{zL}/\sigma_z \approx 1$.

In Fig. 1, the rms heights of the gravity and capillary waves are plotted versus the wind speed u_{10}. In the legend, "Capillary (Bou)" means that K_S is computed from (27), whereas for "Capillary (Elf)," $K_S = 50$ rad/m (value used by Elfouhaily [23]). We can observe that the ratio σ_{zL}/σ_{zS} is much greater than unity (from 16–790) and σ_{zS} computed from our approach (mean value equal to 3.6 mm) has the same order of magnitude as the one obtained for $K_S = 50$ rad/m (mean value equal to 1.1 mm).

In Fig. 2, the correlation lengths in meters of the height L_{c2}, of the skewness L_{c3} [see (24) and according to two approaches] and of the peakedness L_{c4} [see (25)] are plotted, versus the wind speed u_{10}. L_{c2} is computed for $\Phi = 0$ and defined as $W_2(0, \Phi)/W_2(L_{c2}, \Phi) = e^{-1}$. As previously said, the values obtained from the Elfouhaily and our approaches are of the same order of magnitude and decrease with the wind speed. The correlation lengths of the height and the deviated peakedness functions are of the same order of magnitude and increases with the wind speed. Since the correlation lengths of the deviated peakedness and of the height are related to the gravity waves, we have $\{L_{c2}, L_{c4}\}$ much greater than L_{c3}, which is related to
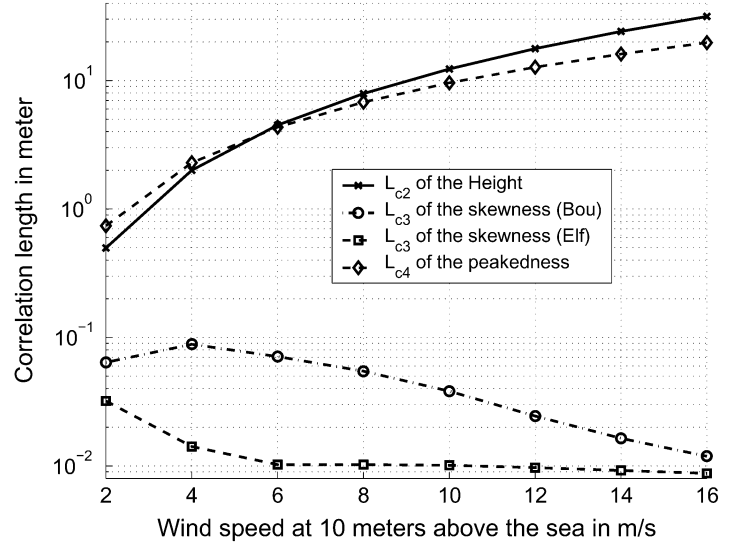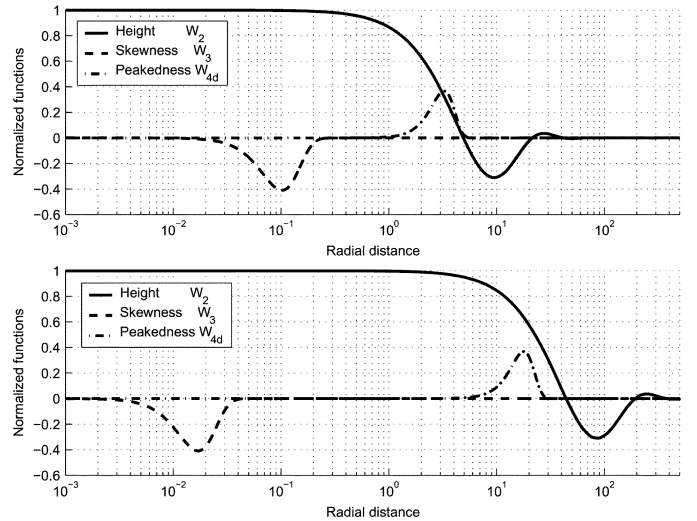

Fig. 3. Normalized correlation functions of the height $W_2(r, \Phi)/\sigma_{zL}^2$, of the skewness $W_3(r, \Phi)/\sigma_{zS}^3$, and of the deviated peakedness $W_{4d}(r)/\sigma_{zL}^4$ versus the radial distance r and for $\Phi = 0$. (Top) Wind speed $u_{10} = 5$ m/s. (Bottom) Wind speed $u_{10} = 15$ m/s.

the capillary waves. This result is in qualitative agreement with the values selected in [7] and found by Guissard [29].

In Fig. 3, the normalized correlation functions of the height $W_2(r, \Phi)/\sigma_{zL}^2$, of the skewness $W_3(r, \Phi)/\sigma_{zS}^3$ and of the deviated peakedness $W_{4d}(r)/\sigma_{zL}^4$ are plotted versus the radial distance r and for $\Phi = 0$. At the top, the wind speed $u_{10} = 5$ m/s and at the bottom, $u_{10} = 15$ m/s. For the height correlation, we can observe that there is a significant range of negative values not present in most of the correlation functions for land surfaces. This comes from the fact that the sea roughness height spectrum reaches to a maximum. The skewness function $W_3(r, \Phi)/\sigma_{zS}^3$ reaches a minimum value equal to $-(3/2)^{3/2} \exp(-3/2) \approx -0.41$, for which the radial distance is $(3/2)^{1/2} L_{c3} \approx 1.22L_{c3}$, whereas $W_{4d}(r)/\sigma_{zL}^4$ reaches a maximum value equal to $e^{-1} = 0.37$, for which the radial distance is L_{c4}.

The Fourier transform of the skewness function $W_3(\mathbf{r})$ is the bispectrum $\hat{W}_3(\mathbf{k})$ and has a simple closed-form in polar coordinates ($\hat{W}_3(\mathbf{k})\,d\mathbf{k} = k \times \hat{W}_3(k,\psi)\,dk\,d\psi$)

$$\hat{W}_3(k,\psi) = -j\frac{\sigma_{zS}^3 L_{c3}^3}{16}k^2 e^{-(\frac{kL_{c3}}{2})^2}[(kL_{c3})^2 - 8]\cos\psi. \quad (28)$$

We can note that $\hat{W}_3(k,\psi)$ is complex without real part. Guissard [29], within the works of Masudo and Kuo [35], pointed out the significance of the imaginary part of the bispectrum. Because of the symmetry properties, it provided no contribution to the third-order moment $\langle z^3 \rangle$. They showed however, through a simple example (e.g., see [29, Fig. 1]), that the waves height are tilted forward or backward depending on the sign of the imaginary part of $\hat{W}_3(k,\psi)$. Thus, the imaginary part of $\hat{W}_3(k,\psi)$ determines the asymmetry of the waves, also called horizontal skewness by Fung [7]. On the other hand, the real part of $\hat{W}_3(k,\psi)$ is related to the vertical skewness; it leads to a wave with sharp peaks and flat troughs, or conversely. This is called vertical skewness in [7]. It yields a skewed displacement of the height distribution (e.g., see [7, Fig. 7A.2]). As shown in the next subsection, since horizontal skewness is asymmetric with respect to the vertical axis, it is the component that influences the difference in the ocean NRBCS in the upwind and downwind directions.

D. Derivation of the Incoherent Scattering Coefficient

In this section, the incoherent scattering coefficient is derived for a bistatic configuration, and the results are simplified for the monostatic case and for microwave frequencies.

1) Bistatic Case: Substituting (8), (22), and (23) into (6), the resulting equation is

$$\langle \exp[jQ(z_2 - z_1)] \rangle = \exp\big[-Q^2\sigma_{zL}^2 + \alpha_0(r) \\ + j\alpha_1(r)\cos(\Phi) - \alpha_2(r)\cos(2\Phi)\big] \quad (29)$$

where

$$\alpha_0(r) = Q^2 W_{20}(r) + Q^4 W_{4d}(r)/2 \quad (30a)$$
$$\alpha_1(r) = Q^3 W_{30}(r) \quad \alpha_2(r) = Q^2 W_{22}(r). \quad (30b)$$

From (1), the incoherent (superscript I) bistatic scattering coefficient is then in polar coordinates (r, Φ)

$$\sigma_{pq}^I(\mathbf{k}_i, \mathbf{k}_s) = \frac{1}{\pi}\left|\frac{2q_i q_s B_{pq}(\mathbf{k}_i, \mathbf{k}_s)}{Q}\right|^2 \exp\big(-Q^2\sigma_{zL}^2\big) \\ \cdot \int_0^\infty r\,dr \int_0^{2\pi} \exp[jk_{si}r\cos(\Phi - \chi)] \\ \cdot \{\exp[\alpha_0(r) + j\alpha_1(r) - \alpha_2(r)\cos(2\Phi)] - 1\}\,d\Phi \quad (31)$$

where

$$\chi = \arctan\left[\frac{(\mathbf{k}_s - \mathbf{k}_i)\cdot\hat{\mathbf{y}}}{(\mathbf{k}_s - \mathbf{k}_i)\cdot\hat{\mathbf{x}}}\right] \quad k_{si} = \|\mathbf{k}_s - \mathbf{k}_i\|. \quad (32)$$

In the backscattering direction, we have

$$Q = 2K_0\cos\theta \quad \chi = \phi \quad k_{si} = 2K_0\sin\theta. \quad (33)$$

In (32), χ is defined from the vectors $\{\mathbf{k}_i, \mathbf{k}_s\}$, where $\mathbf{k}_{i,s} = (k_{ix,sx}, k_{iy,sy}) = (k_{i,s}\cos\phi_{i,s}\sin\theta_{i,s}, k_{i,s}\sin\phi_{i,s}\sin\theta_{i,s})$. In

the backscattering direction, $\mathbf{k}_s = -\mathbf{k}_i$, which implies that $\theta_s = -\theta_i = -\theta$ and $\phi_s = \phi_i = \phi$, where ϕ is the backscattering azimuthal direction along the upwind direction and θ the backscattering incident direction. In (33), K_0 is the incident electromagnetic wavenumber. In most of the articles, excepted in [10] and [13] (where the surface is statistically Gaussian), the angular integration is computed numerically. Thus, $\sigma_{pq}^I(\mathbf{k}_i, \mathbf{k}_s)$ cannot be expanded as a Fourier series along the direction χ. In this paper, the angular integration over Φ is performed analytically, which extends the results obtained in [10] and [13] to a statistically non-Gaussian sea surface. This integration is derived in the Appendix and given by Ψ (45). In addition, to show that Ψ depends only on $\cos(n\chi)$, the sum over n is expanded for $\{n < 0, n = 0, n > 0\}$ and for the case $n < 0$, the variable transformation $n' = -n$ is used. Moreover, the same way is applied for the sum over m. One uses the following properties of the Bessel functions: $J_{-n}(x) = (-1)^n J_n(x), I_{-n}(x) = I_n(x)$, where n is an integer. One then shows

$$\sigma_{pq}^I(\mathbf{k}_i, \mathbf{k}_s) = 2\left|\frac{2q_i q_s B_{pq}(\mathbf{k}_i, \mathbf{k}_s)}{Q}\right|^2 \exp\big(-Q^2\sigma_{zL}^2\big) \\ \cdot \int_0^\infty \exp(\alpha_0)J_0(k_{si}r)r\,dr \left[\Omega_{0,\infty}(\alpha_1, \alpha_2) - 1 \\ + \sum_{n>0} J_n(k_{si}r)\Omega_{n,\infty}(\alpha_1, \alpha_2)\cos(n\chi)\right] \quad (34)$$

where

$$\Omega_{0,M}(\alpha_1, \alpha_2) = J_0(\alpha_1)I_0(\alpha_2) + \sum_{m=1}^{m=M} J_{2m}(\alpha_1)I_m(\alpha_2) \quad (35a)$$

$$\Omega_{n,M}(\alpha_1, \alpha_2) = 2(-1)^n\left\{J_n(\alpha_1)I_0(\alpha_2) \\ + \sum_{m=1}^{m=M}[J_{n+2m}(\alpha_1) \\ + J_{n-2m}(\alpha_1)]I_m(\alpha_2)\right\}. \quad (35b)$$

Thus, the incoherent scattering coefficient is expressed as the sum of even Fourier series according to the angle χ and we can note that there is no component along the harmonics $\sin(n\chi)$. According to the value of $k_{si}r$, the series can be truncated. For instance, around the forward direction defined as $\mathbf{k}_s = \mathbf{k}_i, k_{si} = \|\mathbf{k}_s - \mathbf{k}_i\| \approx 0, J_{n\neq 0}(k_{si}r) \approx 0$ and therefore the incoherent scattering coefficient is independent of the wind direction. On the other hand, in the backscattering direction defined as $\mathbf{k}_s \approx -\mathbf{k}_i$, the incoherent backscattering coefficient depends on the wind direction. The next subsection is devoted to this configuration.

2) Monostatic Case: Bourlier *et al.* [13] considered a Gaussian surface, which means that $\alpha_1 = 0$. Thus, in (35), we have $\Omega_{0,\infty}(0, \alpha_2) = I_0(\alpha_2)$ and $\Omega_{n,\infty}(0, \alpha_2) = 2I_{n/2}(\alpha_2)$ where n is even ($J_m(0) = 0$ for $m \neq 0$). They then showed for radar frequencies $f = \{5.3, 14\}$ GHz and for wind
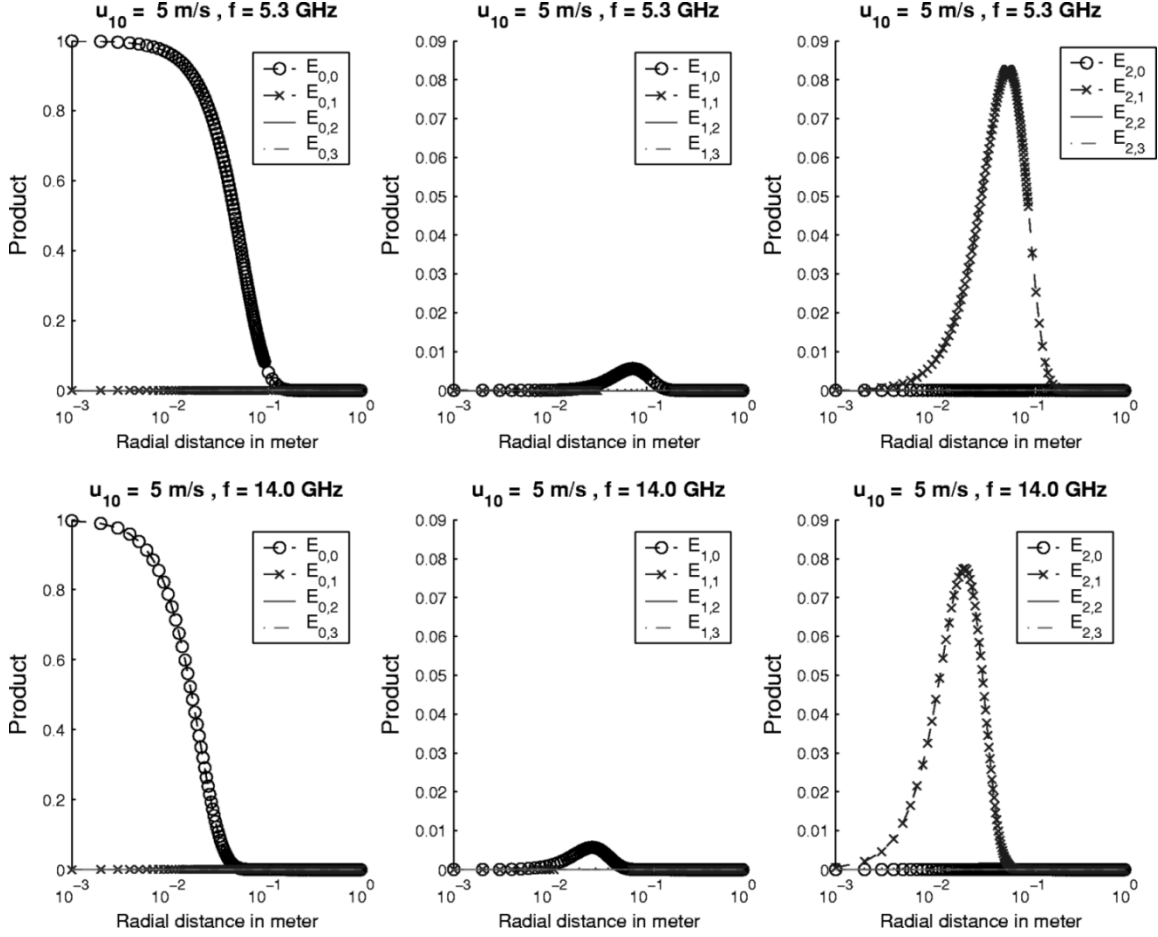
Fig. 4.　Function $E_{n,M}(r) = \exp\{-[Q^2\sigma_{zL}^2 - \alpha_0(r)]\}\Omega_{n,M}(\alpha_1,\alpha_2)$ versus r for $n = \{0,1,2\}$ and $M = \{0,1,2,3\}$. (Top) Wind speed $u_{10} = 5$ m/s. (Bottom) Radar frequencies $f = \{5.3, 14\}$ GHz.

speed $u_{10} = \{5, 15\}$ m/s in the backscattering direction that $\sigma_{pq}^I(\mathbf{k}_i, -\mathbf{k}_i) \approx \sigma_{pq}^{I,0}(\theta) + \sigma_{pq}^{I,2}(\theta)\cos(2\phi)$ and that the higher order coefficients in $\cos(n\phi)$ vanish. Hence, since the non-Gaussian effect of the surface is considered as a small perturbation compared with a surface with Gaussian statistics, the incoherent NRBCR can be expanded up to $n = 2$

$$\sigma_{pq}^I(\mathbf{k}_i, -\mathbf{k}_i) \equiv \sigma_{pq}^I(\theta,\phi) = \sum_{n=0}^{n=2} \sigma_{pq}^{I,n}(\theta)\cos(n\phi) \quad (36)$$

where

$$\sigma_{pq}^{I,0}(\theta) = 2|K_0\cos(\theta)B_{pq}(\mathbf{k}_i, -\mathbf{k}_i)|^2 \exp\left(-Q^2\sigma_{zL}^2\right)$$
$$\cdot \int_0^\infty J_0(k_{si}r)[\exp(\alpha_0)\Omega_{0,\infty}(\alpha_1,\alpha_2) - 1]r\,dr \quad (37a)$$

$$\sigma_{pq}^{I,n}(\theta) = 2|K_0\cos(\theta)B_{pq}(\mathbf{k}_i, -\mathbf{k}_i)|^2 \exp\left(-Q^2\sigma_{zL}^2\right)$$
$$\cdot \int_0^\infty J_n(k_{si}r)\exp(\alpha_0)\Omega_{n,\infty}(\alpha_1,\alpha_2)r\,dr \quad (37b)$$

where $n = \{1,2\}$. Equation (36) is also consistent with experimental data [16], [17] obtained for microwave frequencies, for which the contributions of the higher order harmonics are insignificant.

To study the convergence of the sum according to M, one plots in Fig. 4, the function $E_{n,M}(r) = \exp\{-[Q^2\sigma_{zL}^2 - $

$\alpha_0(r)]\}\Omega_{n,M}(\alpha_1,\alpha_2)$ versus r for $n = \{0,1,2\}$ and $M = \{0,1,2,3\}$, in the backscattering direction where $\theta = 0$ ($k_{si} = 0, Q = 2K_0$) and $\{\alpha_{0,1,2}\}$ are given by (30). The wind speeds $u_{10} = 5$ m/s and the radar frequencies $f = \{5.3, 14\}$ GHz at the top and at the bottom, respectively. We observe that for $M > 1$, the functions vanish and for $E_{0,M}$ the main contribution is given for $M = 0$. Simulations for $u_{10} = 5$ m/s, not reported in this paper, lead to the same conclusion. In (37) the integrand must be multiplied by $J_n(k_{si}r)$ where $k_{si}r = 2rK_0\sin\theta$. Thus, for $\theta > 0, |E_{n,M}(r)| \geq |J_n(k_{si}r)E_{n,M}(r)|$. From (35), $\Omega_{n,\infty}$ can then be simplified as

$$\Omega_{0,\infty}(\alpha_1,\alpha_2) \approx \Omega_{0,0}(\alpha_1,\alpha_2) = J_0(\alpha_1)I_0(\alpha_2) \quad (38a)$$
$$\Omega_{1,\infty}(\alpha_1,\alpha_2) \approx \Omega_{1,1}(\alpha_1,\alpha_2) = 2\{-J_1(\alpha_1)I_0(\alpha_2) \quad (38b)$$
$$+ I_1(\alpha_2)[J_1(\alpha_1) - J_3(\alpha_1)]\},$$
$$\Omega_{2,\infty}(\alpha_1,\alpha_2) \approx \Omega_{2,1}(\alpha_1,\alpha_2) = 2\{+J_2(\alpha_1)I_0(\alpha_2)$$
$$+ I_1(\alpha_2)[J_0(\alpha_1) + J_4(\alpha_1)]\}. \quad (38c)$$

IV. NUMERICAL RESULTS

For incidence angles ($\theta \in [0°, 60°]$) of interest for remote sensing applications and for the VV and HH polarizations, this section presents numerical results of the incoherent NRBCS by assuming a height roughness anisotropic spectrum given
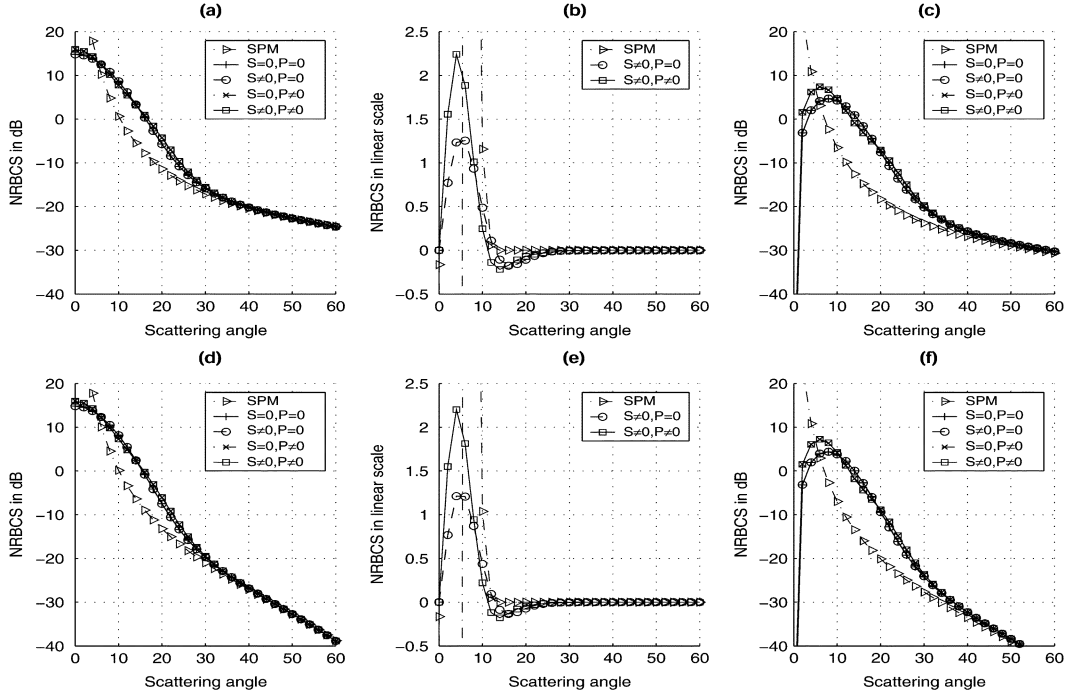
Fig. 5. (Top) VV and (bottom) HH incoherent NRBCS $\{\sigma_{pq}^{I,n}(\theta)\}$ versus the scattering angle for $f = 5.3$ GHz and $u_{10} = 5$ m/s. (a) VV: n = 0. (b) VV: n = 1. (c) VV: n = 2. (d) HH: n = 0. (e) HH: n = 1. (f) HH: n = 2.

by the Elfouhaily *et al.* [25] model. The higher order statistics, like the bicorrelation $W_3(r, \Phi) = W_3(r)\cos\Phi$ [related to the skewness surface and given by (22)] and the tricorrelation $W_{4d}(r)$ [related to the deviated peakedness function and given by (23)] functions, are computed from Section III. The height correlation function $W_2(r, \Phi)$ is computed from the sea height roughness spectrum by using (8) and (9). Two radar frequencies are studied, $f = 5.3$ GHz (C-band, relative permittivity $\epsilon_r = 69 + j35$, [36]) and $f = 14$ GHz (Ku-band, $\epsilon_r = 69 + j35$, [36]). In (37), the terms $\{\sigma_{pq}^{I,n}(\theta)\}$ require the calculation of $\exp\{-[Q^2\sigma_{zL}^2 - \alpha_0(r)]\}$, where $\alpha_0(r) = Q^2 W_{20}(r) + Q^4 W_{4d}(r)/2$. The integral is then convergent if $Q^2\sigma_{zL}^2 - \alpha_0(r) \geq 0$. If $W_{4d} = 0$ ($\alpha_0(r) = Q^2 W_{20}(r)$) then this condition is satisfied for any r, whereas if $W_{4d} \neq 0$, then this condition is not fully satisfied for any r. In fact, W_{4d} is valid for small values of r, which means that W_{4d} is a perturbation compared with $-Q^2\sigma_{zL}^2 + Q^2 W_{20}$. Thus, we can expand $\exp[\alpha_0(r)]$ as $\exp[Q^2 W_{20}(r)][1 + Q^4 W_{4d}(r)/2]$.

A. Coefficients $\{\sigma_{pq}^{I,n}(\theta)\}$ of the Azimuthal Harmonics $\cos(n\phi)$ for $n = \{0, 1, 2\}$

Fig. 5 shows the predictions of the VV and HH incoherent NRBCS $\{\sigma_{pq}^{I,n}(\theta)\}$ in C-band versus the scattering angle for wind speed $u_{10} = 5$ m/s. For the cases (a) and (d), $n = 0$. For the cases (b) and (e), $n = 1$. For the cases (c) and (f), $n = 2$. In the legend, SPM denotes the small perturbation method obtained for $W_{4d} = 0$ (no peakedness), for which

$$\sigma_{pq}^{I,0}(\theta) = \left|B_{pq}^{\mathrm{SPM}}(\mathbf{k}_i, -\mathbf{k}_i)\right|^2 \hat{W}_{20}(K_B) K_B^3 \tag{39a}$$

$$\sigma_{pq}^{I,1}(\theta) = \frac{\cot\theta}{2}\left|B_{pq}^{\mathrm{SPM}}(\mathbf{k}_i, -\mathbf{k}_i)\right|^2 j\hat{W}_{30}(K_B) K_B^4 \tag{39b}$$

$$\sigma_{pq}^{I,2}(\theta) = \sigma_{pq}^{I,0}(\theta)\hat{\Delta}_{20}(K_B) \tag{39c}$$

where

$$K_B = 2K_0\sin\theta \tag{40a}$$

$$\left|B_{pq}^{\mathrm{SPM}}(\mathbf{k}_i, -\mathbf{k}_i)\right|^2 = \frac{\cot^4\theta}{2}\left|B_{pq}(\mathbf{k}_i, -\mathbf{k}_i)\right|^2. \tag{40b}$$

In addition, we have the following:

- $S = 0, P = 0$, means that $W_{30} = 0$ and $W_{4d} = 0$ (no skewness and peakedness);
- $S \neq 0, P = 0$, means that $W_{30} \neq 0$ and $W_{4d} = 0$ (no peakedness);
- $S = 0, P \neq 0$, means that $W_{30} = 0$ and $W_{4d} \neq 0$ (no skewness);
- $S \neq 0, P \neq 0$, means that $W_{30} \neq 0$ and $W_{4d} \neq 0$.

In Fig. 5, we can observe for any polarization that the skewness effect does not affect $\{\sigma_{pq}^{I,n}(\theta)\}$ for $n = 0$ and $n = 2$. Indeed, the levels obtained for $S = 0, P = 0$ and $S = 0, P \neq 0$ are the same as $S \neq 0, P = 0$ and $S \neq 0, P \neq 0$, respectively. This leads from (38) to

$$\Omega_{0,\infty} \approx I_0(\alpha_2) \quad \Omega_{2,\infty} \approx 2I_1(\alpha_2)(\alpha_1 \equiv 0). \tag{41}$$

However, the peakedness effect affects $\sigma_{pq}^{I,0}(\theta)$ (decibel scale) and $\sigma_{pq}^{I,2}(\theta)$ (decibel scale), especially as the wind speed increases and when the scattering angles are close to the nadir. As expected, for scattering angles greater than $30°$ and for any n, for which the Bragg regime is valid, the SPM and the SSA-1 models become similar. In addition, along the scattering angle, the incoherent NRBCS decreases more quickly in HH polarization than in VV polarization. For the coefficient of the first harmonic ($n = 1$), the peakedness phenomenon is not significant (linear scale).

Simulations for $\{u_{10} = 15$ m/s, $f = 5.3$ GHz$\}, \{u_{10} = 5$ m/s, $f = 14$ GHz$\}$, and $\{u_{10} = 15$ m/s, $f = 14$ GHz$\}$, not reported in this paper, lead to the same conclusion. However, we
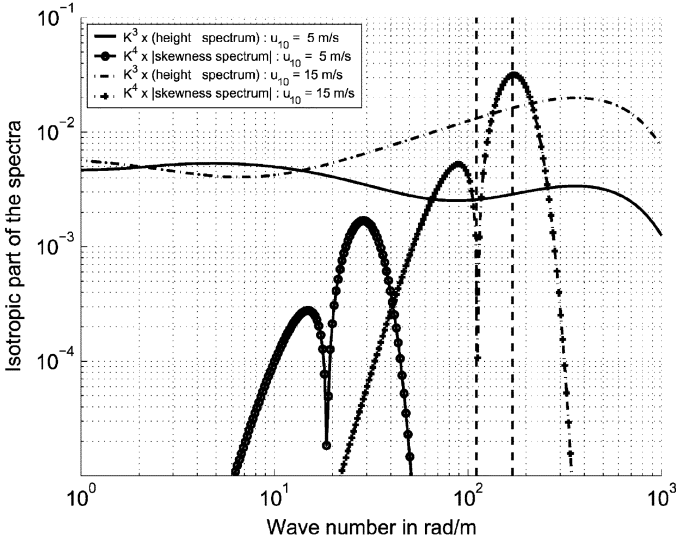
Fig. 6. Isotropic parts of the curvature spectrum $(\hat{W}_{20}(k)k^3)$ and $|j\hat{W}_{30}(k)k^4|$ (modulus of the skewness spectrum multiplied by k^4) versus the wavenumber k for wind speeds $u_{10} = \{5, 15\}$ m/s. The vertical lines represent the value of the Bragg wavenumber $K_B = 2K_0 \sin \theta$ for $f = 5.3$ GHz and $\theta = \{30°, 60°\}$.

could see for $\{u_{10} = 15 \text{ m/s}, f = 5.3 \text{ GHz}\}$ and $n = 1$ that in the Bragg region that the SPM model does not converge toward the SSA-1 model. To explain this disagreement, in Fig. 6 the isotropic parts of the curvature spectrum, $\hat{W}_{20}(k)k^3$, and of $|j\hat{W}_{30}(k)k^4|$ (modulus of the skewness spectrum multiplied by k^4) are plotted versus the wavenumber k for wind speeds $u_{10} = \{5, 15\}$ m/s. The vertical lines represent the value of the Bragg wavenumber $K_B = 2K_0 \sin \theta$ for $f = 5.3$ GHz and $\theta = \{30°, 60°\}$. From (39), in the Bragg region, $\sigma_{pq}^{I;0}(\theta)$ and $\sigma_{pq}^{I;1}(\theta)$ are related to $\hat{W}_{20}(K_B)K_B^3$ and $j\hat{W}_{30}(K_B)K_B^4$, which is real according to (28). We can observe that $|j\hat{W}_{30}(k)k^4|$ reaches zero, obtained from (28) when $(k_0 L_{c3})^2 - 8 = 0 \Rightarrow k_0 = 2^{3/2}/L_{c3} = \{19, 112\}$ rad/m for $u_{10} = \{5, 15\}$ m/s. This means for $k < k_0$ that $j\hat{W}_{30}(k) < 0 \Rightarrow \sigma_{pq}^{I;1}(\theta) < 0$ with SPM, whereas for $k > k_0, j\hat{W}_{30}(k) > 0 \Rightarrow \sigma_{pq}^{I;1}(\theta) > 0$. In the Bragg region, one can observe for $u_{10} = 5$ m/s that the level of $|j\hat{W}_{30}(k)k^4|$ is small comparatively to that obtained for $u_{10} = 15$ m/s. The disagreement between SPM and SSA-1 obtained for $u_{10} = 15$ m/s may come from the fact that in the Bragg region, $|j\hat{W}_{30}(k)k^4|$ is greater than $\hat{W}_{20}(k)k^3$, which means that $\exp(Q^2 W_2 + jQ^3 W_3)$ in (6) cannot be expanded as $1 + Q^2 W_2 + jQ^3 W_3$ to obtain the SPM approximation. Only $\exp(Q^2 W_2)$ can be expanded as $1 + Q^2 W_2$.

B. Comparison of $\{\sigma_{pq}^{I;n}(\theta)\}$ With Experimental Data for $n = \{0, 1, 2\}$ Versus the Scattering Angle

In Fig. 7, the VV and HH incoherent NRBCS $\{\sigma_{pq}^{I;n}(\theta)\}$ are compared with experimental data in C-band [20] (CMOD2-I3) versus the scattering angle ($\theta \in [18°; 58°]$ and there is no experimental data for the HH polarization). At the top, the wind speed $u_{10} = 5$ m/s, whereas at the bottom $u_{10} = 15$ m/s. For the cases (a) and (d), $n = 0$. For the cases (b) and (e), $n = 1$. For the cases (c) and (f), $n = 2$. For $n = \{0, 2\}$ [Fig. 7, cases (a), (c), (d), and (f)], we can observe that the measurement level is larger than the numerical result level. This deviation increases weakly with the

wind speed. For scattering angles $\theta \in [30; 58]$ (corresponding to the range where the SPM model is valid) and for $f = 5.3$ GHz, the Bragg scattering wavenumber is $2K_0 \sin \theta \in [306; 530]$ rad/m. This means for getting a better agreement with the measurement that the sea elevation spectrum must be more important for shorter waves of wavenumber $2K_0 \sin \theta$.

In Fig. 8, the same variation as Fig. 7, is plotted for Ku-band [16] (SASS-II model). For the VV polarization and $n = 0$, one can note a good agreement between the experimental data and the numerical results. As previously mentioned, for the HH polarization in the Bragg region, the numerical curves go below the measurements. A possible explanation of the under estimation of the amplitude of zeroth harmonic at HH polarization is the contribution of the breaking waves. For scattering angles close to the nadir, the measurements coincide with the SSA-1 model for $n = 0$ whereas for $n = 2$, the numerical curves go above the measurements.

In Figs. 7 and 8, for scattering angles smaller than 30°, one can observe that the absolute value of the first harmonic ($n = 1$) of the measurement is small comparatively to that of the numerical results. In fact, the SASS-II model forced $\sigma_{pq}^{I;1}(\theta)$ to be zero at negative values. In the Bragg regime, there is a better agreement between the measurements and the numerical results where the observed level is of the order of 10^{-3} (a zoom of Figs. 7 and 8, of cases (b) and (e), not represented in this paper, allows to evaluate this level). $\sigma_{pq}^{I;1}(\theta)$ is related to the skewness function $W_3(r, \Phi)$ given by (22), where σ_{zS} and L_{c3} have to be determined. Numerical results, not reported in this paper, showed that the level of $\sigma_{pq}^{I;1}(\theta)$ is very sensitive to the value of $\{\sigma_{zS}, L_{c3}\}$, which depend on the wavenumber K_S separating the large and the small scales. For instance, when the value of Elfouhaily et al. is used [23] ($K_S = 50$ rad/m, see Figs. 1 and 2 for the comparison of the Elfouhaily et al. approach with ours), the obtained levels are smaller than ours with a ratio ranging from 2–10, according to the wind speed and the radar frequency. To avoid this problem, Fung and Chen et al. [6], [7], [34] retrieved σ_{zS} and L_{c3} from experimental data. It is not the purpose of this paper, and this point should be investigated in future work.

C. Comparison of $\sigma_{pq}^I(\theta, \phi)$ With Experimental Data Versus the Wind Direction ϕ

In Fig. 9, the VV and HH incoherent NRBCS $\sigma_{pq}^I(\theta, \phi)$ are compared with experimental data in C-band [20] versus the wind direction ϕ. At the top, the wind speed $u_{10} = 5$ m/s, whereas at the bottom $u_{10} = 15$ m/s. For the cases (a) and (c), $\theta = 20°$ whereas for the cases (b) and (d), $\theta = 40°$. The range over ϕ is chosen as $[0; \pi]$ since $\sigma_{pq}^I(\theta, \phi + \pi) = \sigma_{pq}^I(\theta, \phi - \pi)$, which means that $\phi = \pi$ is a symmetry axis. To quantify the skewness effect, we define the variation $\Delta\sigma_{pq}^I(\theta)$ as $\sigma_{pq}^I(\theta, \phi) - \sigma_{pq}^I(\theta, \phi + \pi) = 2\sigma_{pq}^{I;1}(\theta)$.

As shown in Fig. 9 for the numerical results, $0 \leq \Delta\sigma_{pq}^I(\theta) \leq 2$ dB for case (a), $\Delta\sigma_{pq}^I(\theta) \approx 0$ dB for case (b), $-1 \leq \Delta\sigma_{pq}^I(\theta) \leq 0$ dB for case (c), and $0 \leq \Delta\sigma_{pq}^I(\theta) \leq 5$ dB for case (d). If $\Delta\sigma_{pq}^I(\theta) > 0$, then the level is larger in the upwind direction than in the downwind direction and the minimum occurs for $\phi > 90°$. If $\Delta\sigma_{pq}^I(\theta) = 0$, then there is no skewness effect and the minimum occurs in the crosswind
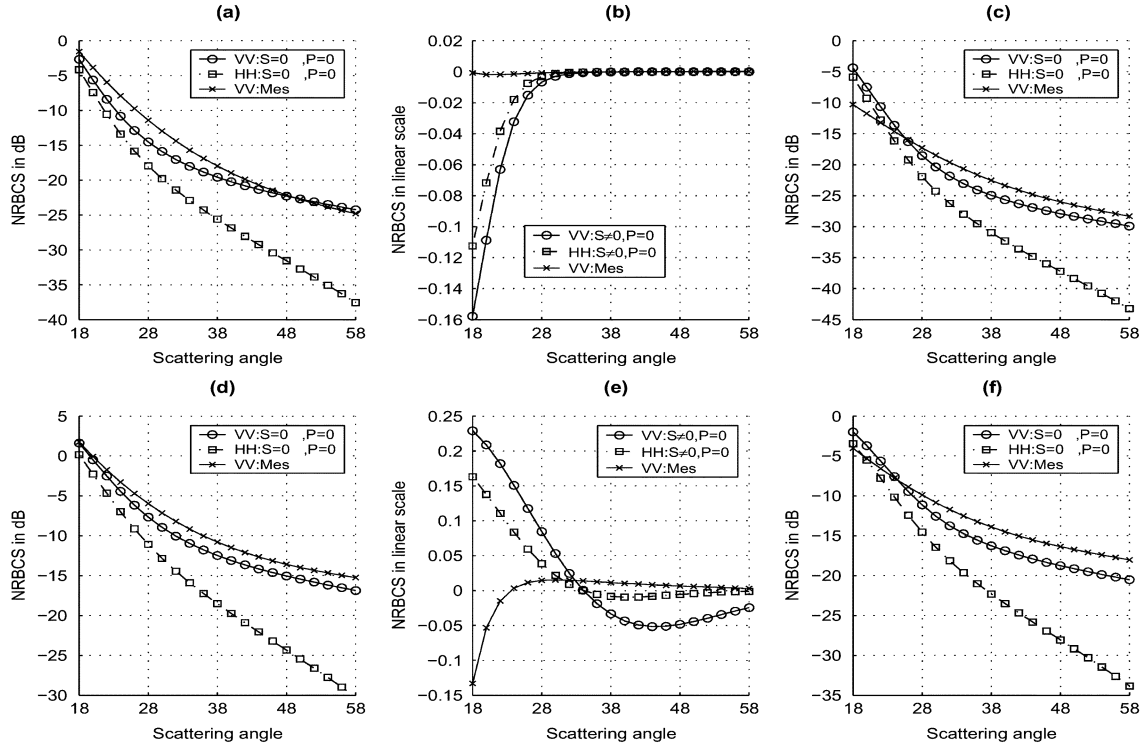
Fig. 7. Comparison of the VV and HH incoherent NRBCS $\{\sigma_{pq}^{I,n}(\theta)\}$ with experimental data in C-band ($f = 5.3$ GHz) versus the scattering angle θ. (a) n = 0, $u_{10} = 5$ m/s, f = 5.3 GHz. (b) n = 1, $u_{10} = 5$ m/s, f = 5.3 GHz. (c) n = 2, $u_{10} = 5$ m/s, f = 5.3 GHz. (d) n = 0, $u_{10} = 15$ m/s, f = 5.3 GHz. (e) n = 1, $u_{10} = 15$ m/s, f = 5.3 GHz. (f) n = 2, $u_{10} = 15$ m/s, f = 5.3 GHz.
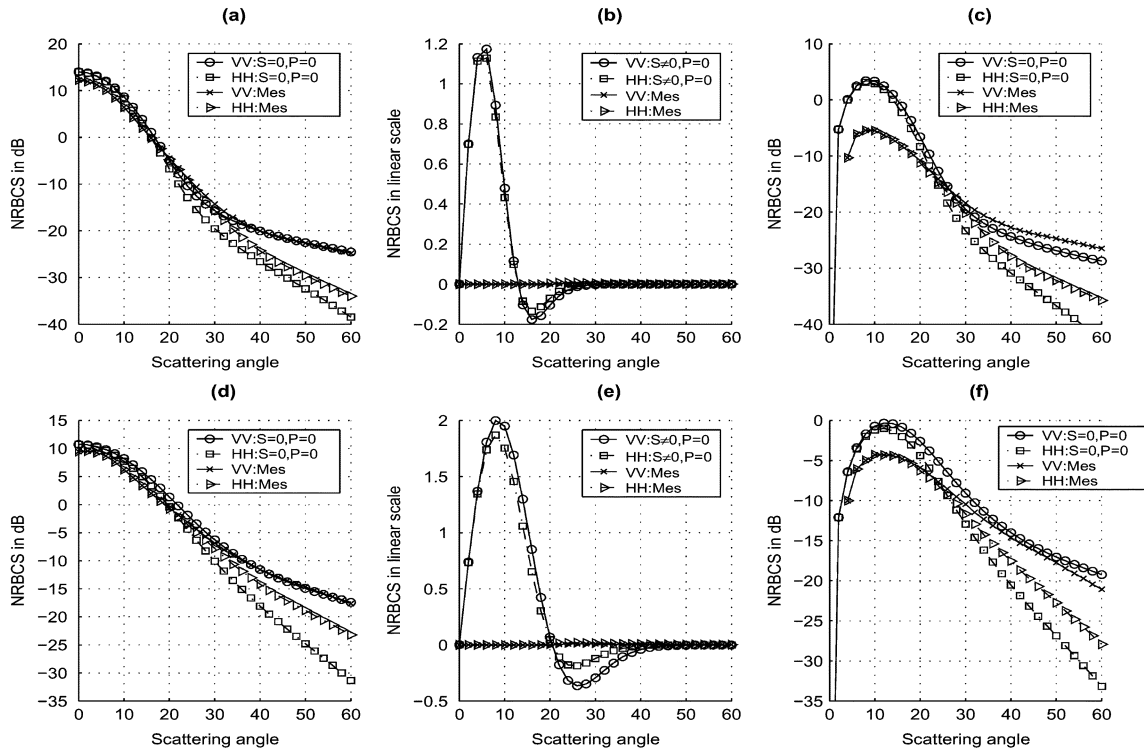

Fig. 8. Same variation as in Fig. 7 for the Ku-band ($f = 14.6$ GHz). (a) n = 0, $u_{10} = 5$ m/s, f = 14.6 GHz. (b) n = 1, $u_{10} = 5$ m/s, f = 14.6 GHz. (c) n = 2, $u_{10} = 5$ m/s, f = 14.6 GHz. (d) n = 0, $u_{10} = 15$ m/s, f = 14.6 GHz. (e) n = 1, $u_{10} = 15$ m/s, f = 14.6 GHz. (f) n = 2, $u_{10} = 15$ m/s, f = 14.6 GHz.

direction ($\phi = 90°$). If $\Delta\sigma_{pq}^{I}(\theta) < 0$, then the level is larger in the crosswind direction than in the upwind direction and the minimum occurs for $\phi < 90°$. The measurements show a

smaller skewness effect than the numerical results. The deviation between the measurements and the numerical results can be explained from Fig. 7. For instance, for case (a) of Fig. 9, the
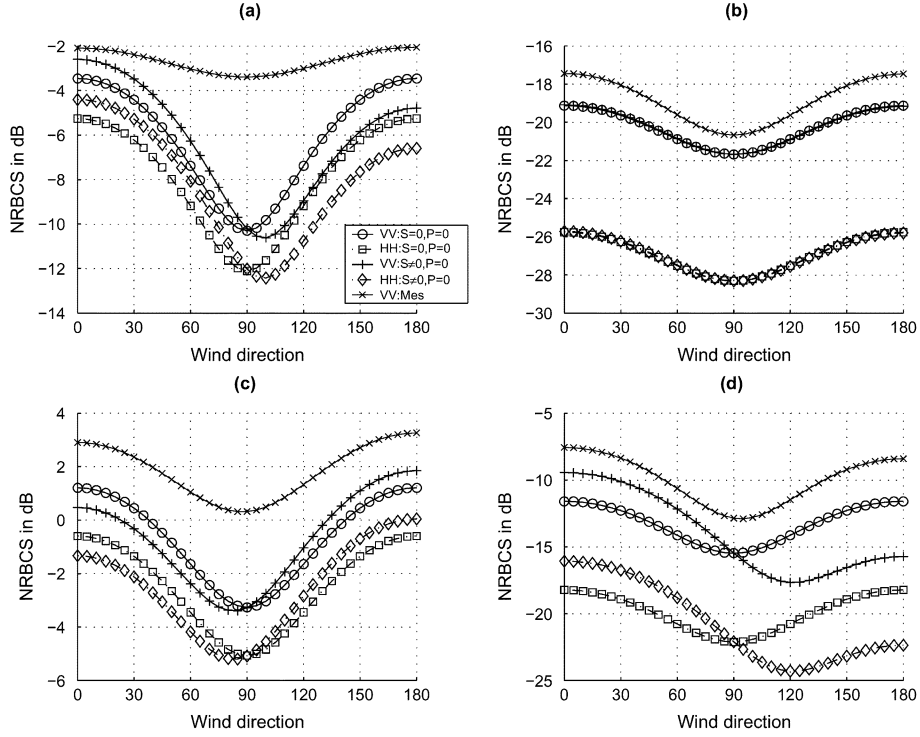
Fig. 9. Comparison of the VV and HH incoherent NRBCS with experimental data in C-band ($f = 5.3$ GHz) versus the wind direction ϕ. (a) $\theta = 20°$, $u_{10} = 5$ m/s, f = 5.3 GHz. (b) $\theta = 40°$, $u_{10} = 5$ m/s, f = 5.3 GHz. (c) $\theta = 20°$, $u_{10} = 15$ m/s, f = 5.3 GHz. (d) $\theta = 40°$, $u_{10} = 15$ m/s, f = 5.3 GHz.

maximum deviation is about 6 dB and occurs for $\phi = 90°$, since for $\theta = 20°$ we observe in Fig. 7(c) a deviation of the order of 5 dB. Similar simulation for $f = 14.6$ GHz, not reported in this paper, lead to the same conclusions. We have shown that if $k < k_0 = 2^{3/2} L_{c3}$ then $j\hat{W}_{30}(k) < 0$, which means that $\Delta\sigma_{pq}^I(\theta) < 0$ by assuming that the SPM is valid. This remark suggests us that the sign of $\Delta\sigma_{pq}^I(\theta)$ is related to L_{c3}.

V. CONCLUSION

In this paper, the incoherent normalized radar backscattering cross section NRBCS is calculated from the first-order small slope approximation by considering non-Gaussian statistics of the sea surface. The NRBCS is then expanded as an even Fourier series in $\cos(n\phi)$ (where n is a positive integer), which can be truncated up to the second order for microwave frequencies and moderate wind speeds. The azimuthal harmonic coefficients demand then only the computation of a one-dimensional integral over the radial distance. The second-order statistics are obtained from the Elfouhaily *et al.* surface height roughness spectrum, whereas the third (related to the skewness effect) and the fourth (related to the peakedness or kurtosis effect) order statistical moments are computed from the Cox and Munk slope distribution for radial distances close to zero. In addition, for any radial distance, the corresponding correlation functions are assumed, which have to obey symmetry properties expressed in the spatial domain. Thanks to the skewness effect, the up-wind/downwind asymmetry of the incoherent NRBCS is predicted, whereas the upwind/crosswind asymmetry is predicted from the height roughness spectrum.

Comparisons of experimental data in C- and Ku-bands with the zero- and second-order harmonic coefficients show a rela-

tively good agreement. As shown in [10] and [12], better agreement with measurements could be obtained by modifying the sea height roughness spectrum. The modification means a more directional spectrum for long waves (at near-nadir scattering angles, the magnitude of the second-order azimuthal harmonic decreases), and a less directional spectrum for shorter waves (in the Bragg regime, the magnitude of second-order azimuthal harmonic increases). For the first-order azimuthal harmonic, there is a poor agreement between the numerical results and the experimental data. In fact, we have shown that the numerical results are very sensitive to the skewness correlation length. This parameter is difficult to compute because there are poor experimental data in the literature. However, we have shown that the variation $\Delta\sigma_{pq}^I(\theta)$, defined as $\sigma_{pq}^I(\theta, \phi) - \sigma_{pq}^I(\theta, \phi + \pi) = 2\Delta\sigma_{pq}^{I,1}(\theta)$, is related to the sign of the minus of the imaginary part of the skewness spectrum. To avoid this problem, Fung and Chen *et al.* retrieved this parameter from experimental data. This point should be investigated in future work.

APPENDIX

We need to solve the following integral over Φ

$$\Psi(a, \alpha_1, \alpha_2, \chi) = \frac{1}{2\pi} \int_0^{2\pi} \exp[ja\cos(\Phi - \chi) + j\alpha_1 \cos\Phi - \alpha_2 \cos(2\Phi)]\, d\Phi. \quad (42)$$

The complex exponential can be expressed as [37]

$$\begin{cases} e^{ja\cos(\Phi-\chi)} = \sum_{n=-\infty}^{n=+\infty} j^n J_n(a) e^{jn(\Phi-\chi)} \\ e^{-\alpha_2 \cos(2\Phi)} = \sum_{m=-\infty}^{m=+\infty} j^m J_m(j\alpha_2) e^{2jm\Phi} \\ e^{j\alpha_1 \cos(\Phi)} = \sum_{p=-\infty}^{p=+\infty} j^p J_p(\alpha_1) e^{jp\Phi} \end{cases} \quad (43)$$

where J_m is the Bessel function of the first kind and of order m. Substituting (43) into (42) and performing the integration over Φ, we show

$$\Psi = \sum_{n,m,p} j^{n+m+p} J_n(a) J_m(j\alpha_2) J_p(\alpha_1) e^{-jn\chi} \delta_{0,p+n+2m}$$

(44)

where δ_{ij} is the Kronecker symbol defined as $\delta_{ij} = 1$ if $i = j$ else 0. Using the relation $J_m(j\alpha_2) = j^m I_m(\alpha_2)$ where I_m denotes the Bessel function of the second kind and of order m, we obtain

$$\Psi = \sum_{n,m} J_n(a) I_m(\alpha_2) J_{-n-2m}(\alpha_1) e^{-jn\chi}.$$ (45)

REFERENCES

[1] B. Semyonov, "Approximate computation of scattering electromagnetic waves by rough surface contour," *Radio Eng. Electron. Phys.*, vol. 11, pp. 1179–1187, 1966.

[2] A. K. Fung and K. K. Lee, "A semi-empirical sea-spectrum model for scattering coefficient estimation," *IEEE J. Oceanic Eng.*, vol. OE-4, pp. 166–176, 1982.

[3] F. T. Ulaby, R. K. Moore, and A. K. Fung, *Microwave Remote Sensing*, MA: Addison-Wesley, 1982, vol. II.

[4] W. J. Plant, "A two scale model for short wind-generated waves and scatterometry," *J. Geophys. Res.*, vol. 91, no. C9, pp. 10735–10749, 1986.

[5] N. I. Nickolaev, O. I. Yordanov, and M. A. Michalev, "Non-Gaussian effects in the two-scale model for rough surface scattering," *J. Geophys. Res.*, vol. 97, no. C10, pp. 15617–15624, 1992.

[6] K. S. Chen, A. K. Fung, and D. E. Weissman, "A backscattering model for ocean surface," *IEEE Trans. Geosci. Remote Sensing*, vol. 30, pp. 811–817, July 1992.

[7] A. K. Fung, *Microwave Scattering and Emission Models and Their Applications*. Boston, MA: Artech House, 1994.

[8] J. L. Alvarez-Pérez, "An extension of the IEM/IEMM surface scattering model," *Waves Random Media*, vol. 11, no. 3, pp. 307–329, 2001.

[9] A. G. Voronovich, *Wave Scattering from Rough Surfaces*, 2nd ed, ser. Springer Series on Wave Phenomena. Berlin, Germany: Springer-Verlag, 1999.

[10] V. Voronovich, U. Zavorotny, and V. G. Irisov, "Sea-roughness spectrum retrieval from radar and radiometric measurements," in *Proc. IGARSS*, 2000, pp. 3102–3104.

[11] A. G. Voronovich and V. U. Zavorotny, "Theoretical model for scattering of radar signals in Ku- and C-bands from a rough sea surface with breaking waves," *Waves Random Media*, vol. 11, pp. 247–269, 2001.

[12] S. T. McDaniel, "Small-slope predictions of microwave backscatter from the sea surface," *Waves Random Media*, vol. 11, pp. 343–360, 2001.

[13] C. Bourlier and G. Berginc, "Microwave analytical backscattering models from randomly rough anisotropic sea surface—Comparison with experimental data in C and Ku bands," in *Progress in Electromagnetic Research*, Y. Zhang and T. M. Grzegorczyk, Eds. Cambridge, MA: EMW, 2002, vol. 37, pp. 31–78.

[14] T. Elfouhaily, S. Guignard, R. Awadallah, and D. R. Thompson, "Local and nonlocal curvature approximation: A new asymptotic theory for wave scattering," *Waves Random Media*, vol. 13, pp. 321–337, 2003.

[15] S. T. McDaniel, "Microwave backscatter from non-Gaussian seas," *IEEE Trans. Geosci. Remote Sensing*, vol. 41, pp. 811–817, Jan. 2003.

[16] F. J. Wentz, S. Peteherich, and L. A. Thomas, "A model function for ocean radar cross section at 14.6 GHz," *J. Geophys. Res.*, vol. 89, pp. 3689–3704, 1984.

[17] M. Masuko, K. Okamoto, M. Shimada, and S. Niwa, "Measurements of microwave bsckscattering signatures of the oecan surface using X band and Ka band airbone scatterometers," *J. Geophys. Res.*, vol. 91, no. C11, pp. 13065–13088, 1986.

[18] S. V. Nghiem, F. K. Li, and G. Neumann, "The dependence of ocean backscatter at Ku-band on oceanic and atmospheric parameters," *IEEE Trans. Geosci. Remote Sensing*, vol. 35, pp. 581–600, May 1997.

[19] Y. Quilfen, B. Chapron, T. Elfouhaily, K. Katsaros, and J. Tournadre, "Observation of tropical cyclones by high resolution scatterometry," *J. Geophys. Res.*, vol. 103, pp. 7767–7786, 1998.

[20] A. Bentamy, P. Queffeulou, Y. Quilfen, and K. Katsaros, "Ocean surface wind fields estimated from satellite active and passive microwave instruments," *IEEE Trans. Geosci. Remote Sensing*, vol. 37, pp. 2469–2486, Sept. 1999.

[21] F. J. S. Wentz and D. K. Smith, "A model function for ocean-normalized radar cross section at 14 GHz derived from NSCAT observations," *J. Geophys. Res.*, vol. 104, no. C5, pp. 11499–11514, 1999.

[22] M. S. Longuet-Higgins, "The effect of nonlinearities on statistical distributions in the theory of sea waves," *J. Fluid Mech.*, vol. 17, pp. 459–480, 1963.

[23] T. M. Elfouhaily, "A consistent wind and wave model and its application to microwave remote sensing of the ocean surface," Thesis dissertation in English, Denis Diderot Univ., Paris, France, 1997.

[24] C. Cox and W. Munk, "Statistics of the sea surface derived from sun glitter," *J. Mar. Res.*, vol. 13, pp. 198–226, 1954.

[25] T. Elfouhaily, B. Chapron, K. Katsaros, and D. Vandemark, "A unified directional spectrum for long and short wind-driven waves," *J. Geophys. Res.*, vol. 102, no. C7, pp. 781–796, 1997.

[26] E. I. Thorsos and S. L. Broschat, "An investigation of the small slope approximation for scattering from rough surfaces. Part I. Theory," *J. Acoust. Soc. Amer*, vol. 97, no. 4, pp. 2082–2093, 1995.

[27] S. L. Broschat and E. I. Thorsos, "An investigation of the small slope approximation for scattering from rough surfaces. Part II. Numerical studies," *J. Acoust. Soc. Amer*, vol. 101, no. 5, pp. 2615–2625, 1997.

[28] G. Berginc, "Small-slope approximation method: A further study of vector wave scattering from two-dimensional surfaces and comparison with experimental data," in *Progress in Electromagnetic Research*, Y. Zhang and T. M. Grzegorczyk, Eds. Cambridge, MA: EMW, 2002, vol. 37, pp. 251–287.

[29] A. Guissard, "Multispectra in rough surface scattering with applications to the ocean surface," *J. Electromagn Waves Appl.*, vol. 10, no. 10, pp. 1413–1448, 1996.

[30] C. Bourlier, J. Saillard, and G. Berginc, "Study of the sea behavior," in *Progress in Electromagnetic Research*, J. A. Kong, Ed. Cambridge, MA: EMW, 2000, vol. 27, pp. 193–225.

[31] S. Wenying, S. T. P. Charlock, and K. Rutledge, "Observations of reflectance distribution around sunglint from a coastal ocean platform," *Appl. Opt.*, vol. 41, no. 35, pp. 7369–7383, 2002.

[32] M. S. Longuet-Higgins, "On the skewness of the sea surface slopes," *J. Phys. Oceanogr.*, vol. 12, pp. 1283–1291, 1982.

[33] A. K. Fung and K. S. Chen, "Kirchhoff model for a skewed random surface," *J. Electromagn. Waves Appl.*, vol. 5, no. 2, pp. 205–216, 1991.

[34] K. S. Chen, A. K. Fung, and F. Amar, "An empirical bispectrum model for the sea surface scattering," *IEEE Trans. Geosci. Remote Sensing*, vol. 31, pp. 830–835, July 1993.

[35] A. Masuda and Y. Y. Kuo, "A note on the imaginary part of bispectra," *Deep-Sea Res.*, vol. 28A, no. 3, pp. 213–222, 1981.

[36] W. Ellison, A. Balana, G. Delbos, K. Lamkaouchi, L. Eymard, C. Guillou, and C. Prigent, "New permittivity measurements of seawater," *Radio Sci.*, vol. 33, pp. 639–648, 1998.

[37] *Handbook of Mathematical Functions*, Dover, New York, 1972. M. Abramowitz, I. A. Segun.

Christophe Bourlier was born in La Flèche, France on July 6, 1971. He received the "Electronic" DEA (Diplôme d'étude Approfondie) degree from the University of Rennes, Rennes, France, in 1995. While at the University of Rennes, he was with the Laboratory of Radiocommunication, where he worked on antennas coupling in the VHF-HF band. He received the Ph.D. degree in 1999 from the Institut de Recherche et d'Enseignement Supèrieur aux Techniques de l'Electronique, Nantes, France.

He is currently with the Institut de Recherche en Electrotechnique et Electronique de Nantes Atlantique, Nantes, France, working in the radar team located at Ecole polytechnique de l'université de Nantes. He works as a Researcher of the Centre National de la Recherche Scientifique on the problem of electromagnetic wave scattering from rough surfaces in microwave and infrared bands. He is author of more than 40 journal articles and conference papers.